HHS Public Access

Author manuscript

Aerosol Sci Technol. Author manuscript; available in PMC 2023 December 06.

Published in final edited form as:

Aerosol Sci Technol. 2022 ; 56(12): 1146–1155. doi:10.1080/02786826.2022.2128712.

Comparison of the survival of different isolates of SARS-CoV-2 in evaporating aerosols

P. A. Dabisch,

S. P. Wood,

B. P. Holland,

J. A. Boydston,

K. E. Beck,

B. Green,

J. Biryukov

National Biodefense Analysis and Countermeasures Center, Operated by Battelle National Biodefense Institute for the US Department of Homeland Security Science and Technology Directorate, Frederick, Maryland, USA

Abstract

Numerous variants of SARS-CoV-2 with increased transmissibility have emerged over the course of the pandemic. Potential explanations for the increased transmissibility of these variants include increased shedding from infected individuals, increased environmental stability, and/or a lower infectious dose. Upon exhalation of a respiratory particle into the environment, water present in the particle is rapidly lost through evaporation, resulting in a decrease in particle size. The aim of the present study was to compare the losses of infectivity of different isolates of SARS-CoV-2 during the rapid evaporation of aerosol particles that occurs immediately post-generation to assess if there are differences suggestive of increased survival, and ultimately greater transmissibility, for more recent variants. Losses of infectivity of several isolates of SARS-CoV-2 suspended in viral culture media were assessed following aerosolization and evaporation in a flowing chamber. The results demonstrate that losses of infectivity measured post-evaporation were similar for three different isolates of SARS-CoV-2, including isolates from the more recent Delta and Omicron

CONTACT Paul Dabisch, paul.dabisch@st.dhs.gov, National Biodefense Analysis and Countermeasures Center, Operated by Battelle National Biodefense Institute for the US Department of Homeland Security Science and Technology Directorate, 8300 Research Plaza, Frederick, MD 21701, USA.

lineages. The average loss in infectivity across all three isolates was 61 ± 15% (−0.46 ± 0.17 $\log_{10}$ $TCID_{50}$/L-air) at a relative humidity <30%. These results, together with those from several previous studies, suggest that it is unlikely that an increase in environmental stability contributes to the observed increases in transmissibility observed with more recent variants of SARS-CoV-2.

Introduction

Infectious SARS-CoV-2 and viral RNA have been detected in exhaled breath samples and in air samples collected in the vicinity of infected individuals (Adenaiye et al. 2022; Lednicky et al. 2020, 2021; Ma et al. 2021), suggesting that particles generated from the respiratory tract play a role in the transmission of COVID-19. Particles are generated from the fluid lining the respiratory tract during different activities, including breathing, speaking, and coughing. The number and size of these particles is influenced by the specific respiratory activity, with activities such as speaking or coughing generating both greater quantities and larger particles than quiet breathing. Upon exhalation into the environment, water present in the particle is rapidly lost through evaporation, resulting in a decrease to a new equilibrium particle size post-exhalation (Bourouiba 2020; Bourouiba, Dehandschoewercker, and Bush 2014; Liu et al. 2017; Nicas, Nazaroff, and Hubbard 2005; Figure 1).

Throughout the COVID-19 pandemic, numerous variants of SARS-CoV-2 with increased transmissibility have emerged. Potential explanations for the increased transmissibility include increased shedding of virus from infected individuals (Adenaiye et al. 2022; Bolze et al. 2021; Li et al. 2022; Moreira et al. 2021; Teyssou, Delagrèverie, et al. 2021; Teyssou, Soulie, et al. 2021), increased environmental survival during transport from an infected host to an uninfected individual, and/or a decrease in the amount of virus needed to cause infection in a susceptible individual.

Numerous studies have investigated the loss of infectivity of SARS-CoV-2 in aerosol particles that have equilibrated with the ambient environment (Dabisch, Schuit, et al. 2021; Schuit et al. 2021; Schuit et al. 2020; Smither et al. 2020; van Doremalen et al. 2020). These studies have demonstrated that under typical indoor conditions (~20 °C, 20–60% RH, no UV radiation), the virus can remain infectious in aerosol particles for extended periods of time, providing further support for a role of aerosols in transmission (Dabisch, Schuit, et al. 2021; Schuit et al. 2020; Smither et al. 2020). Under some environmental conditions, such as higher temperatures and in the presence of simulated sunlight, the loss of viral infectivity is more rapid, with only a few minutes needed to inactivate 90% of infectious virus (Dabisch, Schuit, et al. 2021; Schuit et al. 2020). Our laboratory recently reported that the decay rates of different isolates of SARS-CoV-2 in equilibrated aerosols were similar across a range of different environmental conditions (Schuit et al. 2021). This result, coupled with the already low decay rates measured for equilibrated aerosols under indoor conditions, suggest that the increased transmissibility observed with more recent variants is unlikely to be due to an increase in the stability of the virus in equilibrated aerosols.

Numerous studies have suggested that microorganisms in aerosols can be damaged in the period immediately after generation as a particle evaporates and equilibrates with the ambient environment (Benbough 1967; Ferry, Brown, and Damon 1958; Hess 1965;

Schaffer, Soergel, and Straube 1976; Theunissen et al. 1993; Wathes, Howard, and Webster 1986; Webb 1959; Xie et al. 2006). It has been recently reported that the infectivity of aerosolized SARS-CoV-2 decreased significantly during the rapid evaporation that occurs immediately following particle generation (Oswin et al. 2022). This study utilized an electrodynamic balance to trap particles for defined periods of time and under controlled humidity levels and demonstrated that 50–60% of infectious virus was inactivated within the first few minutes following particle generation at relative humidity (RH) levels below 50%, with lesser degrees of inactivation observed at RH levels >60%. The observed loss was similar for several viral isolates from earlier in the pandemic, including the Alpha and Beta variants, suggesting that differences in the survival of different viral isolates during this rapid evaporation are unlikely to be responsible for the observed differences in transmissibility between variants.

The aim of the present study was to compare the losses of infectivity of different isolates of SARS-CoV-2, including isolates from the more recent Delta and Omicron lineages, during the rapid evaporation of aerosol particles that occurs immediately post-generation to assess if there are differences suggestive of increased survival that could contribute to the greater transmissibility observed for more recent variants. The results complement those of Oswin et al. (2022), namely that a significant fraction of aerosolized virus loses infectivity during the rapid evaporation that occurs immediately following particle generation, and extends this finding to include more recent variants of SARS-CoV-2, providing additional evidence that increased environmental survival is unlikely to be a significant factor contributing to the increased transmissibility associated with more recent viral variants.

Materials and methods

Testing was performed with multiple isolates of SARS-CoV-2, including the prototype virus (hCoV-19/USA/WA-1/2020, NR-53872, BEI Resources), the Delta variant (hCoV-19/USA/PHC658/2021; NR-55612, BEI Resources), and the Omicron variant (hCoV-19/USA/MD-HP20874/2021, NR-56462, BEI Resources). All viral stocks were provided by NIAID through BEI Resources. Stocks were between passage 3 and passage 4, and were initially passaged in cells of Vero lineage followed by a single passage in Calu-3 cells. Viral stocks were not passaged further following receipt from BEI Resources prior to use. All viral stocks were stored at −80 °C in Eagle's minimum essential medium (EMEM) supplemented with 2% fetal bovine serum until use. The sequence submissions in GISAID for hCoV-19/USA/WA-1/2020 and hCoV-19/USA/MD-HP20874/2021 (Omicron) are EPI_ISL_404895 and EPI_ISL_7160424, respectively. Sequence information for hCoV-19/USA/PHC658/2021 (Delta) is available in GenBank (OL442162).

The concentration of infectious virus in each stock was estimated using a Vero cell-based (ATCC CCL-81) microtitration assay as described in detail previously (Dabisch, Biryukov, et al. 2021; Schuit et al. 2021; Schuit et al. 2020) and reported as median tissue culture infectious doses ($TCID_{50}$) per mL. Microtitration assay plates were read between four- and seven-days post infection, as preliminary testing indicated that there were not significant differences between viral titers measured on different days in this timeframe. The initial concentrations of infectious virus for the prototype virus (hCoV-19/USA/WA-1/2020),

the Delta variant (hCoV-19/USA/PHC658/2021), and the Omicron variant (hCoV-19/USA/MD-HP20874/2021) were 5.5 $\log_{10}$ $TCID_{50}$/mL, 4.6 $\log_{10}$ $TCID_{50}$/mL, and 4.2 $\log_{10}$ $TCID_{50}$/mL, respectively.

Aerosol generation and sampling of virus occurred in a cylindrical polycarbonate chamber with a total volume of 67.5 L (Figure 2). Aerosol generation occurred using an air assist nozzle (IAZA5200415K, The Lee Company) attached to the top of the chamber. The nozzle was supplied with dry compressed air at 55–60 psi, resulting in an output of 16–17 L/min of air at 5–6% RH. For aerosol generation, the nozzle was supplied with viral suspension at 0.05 mL/min, resulting in an increase in the RH of the output air to ~25% RH once the supplied suspension evaporated. Humidity controlled dilution air at a similar RH to the nozzle output (20–25% RH; 40 L/min), controlled by mixing dry compressed air with humidified air generated using a Nafion bundle (FC125-240-5MP; PermaPure), was supplied from four ports located around the aerosol generation nozzle. Temperature and humidity were measured by probes located at the proximal and distal ends of the chamber (HMP110, Vaisala). The average temperature and relative humidity levels measured at the proximal and distal ends of the chamber were within 1 °C and 1% RH of each other. The average temperature and relative humidity (RH) across all tests with virus were 24.8 ± 1.2 °C and 23.6 ± 2.3%, respectively. The low RH level utilized was chosen to help ensure evaporation of the generated particles, and was not meant to mimic a specific environment.

The initial droplet size distribution produced by the nozzle with the aforementioned settings and water had a volume median diameter (VMD) of 6.3 ± 0.2 μm with a geometric standard deviation (GSD) of 1.46 ± 0.02, measured using a phase Doppler particle analyzer (PDPA; TSI Inc.). The particle size distribution measured with water is expected to be representative of that produced with viral culture medium as the viscosity and surface tension of the viral suspension medium are similar to that of water (Additional details provided in Supplementary Information).

For each test, SARS-CoV-2 was aerosolized for five minutes. SARS-CoV-2 isolates were supplied in EMEM supplemented with 2% heat-inactivated fetal bovine serum (FBS). An additional set of tests was conducted to examine the influence of protein content on viral survival during evaporation. These tests utilized SARS-CoV-2 WA-1 diluted in culture media for growth (gMEM), consisting of Minimum Essential Medium (MEM; 11095-098, Gibco) with 10% FBS (12107 C, Atlanta Biologicals), 2 mM GlutaMAX (35-050-061, Life Technologies), 0.1 mM nonessential amino acid (NEAA; 11140-050, Life Technologies), 1 mM sodium pyruvate (11360-070, Life Technologies), and 1% antibiotic-antimycotic solution (15240-062, Life Technologies).

The generated aerosols were sampled from ports located at the distal end of the chamber. Sampling consisted of two individual 25-mm polytetrafluoroethylene (PTFE) filters (225-3708, SKC Inc.) in open-face Delrin filter holders (1107, Pall) flowing at 5 L/min and an Aerodynamic Particle Sizer (APS; Model 3321, TSI Inc.) with a 1:100 diluter (Model 3302 A, TSI Inc.) flowing at 5 L/min. An additional 40 L/min of exhaust flow was pulled from a separate HEPA-filtered port, resulting in a total exhaust flow of 55 L/min. Based on the chamber air flow rate and volume, the average particle residence time in the

chamber was between 60 and 90 s. A HEPA filtered port located at the proximal end of the chamber prevented pressurization of the system due to the small imbalance between the supply and exhaust air flows.

Aerosol sampling started at the beginning of aerosol generation and ended five minutes after the end of aerosol generation, for a total sampling duration of ten minutes. At the end of the sampling period, filters were removed from their holders, placed in a 50-mL conical tube containing 5 mL of gMEM, and vortexed to re-suspend collected aerosol. Viral infectivity of the re-suspended sample was assessed using a microtitration assay (Schuit et al. 2021; Schuit et al. 2020). Four replicate tests were conducted with each SARS-CoV-2 isolate.

The measured average aerosol concentration of infectious virus ($C_{v,m}$), expressed as $\log_{10}$ $TCID_{50}$/L-air, was calculated as the ratio of the amount of infectious virus recovered from the filter to the amount of air sampled using Equation (1), where $C_{v,sample}$ is the concentration of infectious virus in a recovered filter sample, V_{sample} is the volume of gMEM utilized to re-suspend material collected on filter samples, $Q_{sampler}$ is the sampler air flow rate, and $t_{sampling}$ is the sampling duration.

$$C_{v,m} = \log_{10}\left(\frac{C_{v,sample} * V_{sample}}{Q_{sampler} * t_{sampling}}\right) \quad (1)$$

The expected average aerosol concentration of infectious virus ($C_{v,e}$), expressed as $\log_{10}$ $TCID_{50}$/L-air, was calculated as the ratio of the amount of virus aerosolized to the total volume of air flowing through the system during the sampling period, normalized for physical losses, using Equation (2), where $C_{v,stock}$ is the concentration of infectious virus in the suspension aerosolized, Q_{nozzle} is the liquid feed rate to the nozzle, $t_{generation}$ is the generation duration, Q_{system} is the total air flow rate of the system, $t_{sampling}$ is the sampling duration, and η_p is the physical transport efficiency of the system.

$$C_{v,e} = \log_{10}\left(\frac{C_{v,stock} * Q_{nozzle} * t_{generation}}{Q_{system} * t_{sampling}} * \eta_p\right) \quad (2)$$

The physical transport efficiency of the system (η_p) was estimated in a separate set of tests. For these tests, aerosols were generated from sodium fluorescein salt (46960-25 G-F, Millipore Sigma) dissolved in phosphate buffered saline (#10010023, ThermoFisher Scientific) as a physical tracer. Aerosols generated with the tracer had similar mass median aerodynamic diameter (MMAD) and geometric standard deviation (GSD) values as viral aerosols. The average η_p for these tests was 58.4 ± 4.8% (n = 6). These tests also demonstrated that the aerosol concentration was uniform between the two filter sampling ports and the exhaust port. Additional details of this testing are provided in the Supplementary Information.

Losses of infectious virus in the system were estimated as the difference between the $\log_{10}$ concentration of infectious virus measured by filter samplers ($C_{v,m}$) to the expected $\log_{10}$ concentration based on the amount of virus aerosolized and the physical transport efficiency of the system ($C_{v,e}$) (Equation 3).

$$\text{Loss of viral infectivity}\left(\log_{10}\frac{\text{TCID}_{50}}{\text{L}-\text{air}}\right) = C_{v,m} - C_{v,e} \quad (3)$$

Any losses in viral infectivity observed in the test system could occur during aerosol generation, during the rapid evaporation that occurs immediately post-evaporation, or during the sampling process. To assess potential losses during aerosol generation as viral suspension passes through the nozzle and is atomized, but before evaporation can occur, the output of the nozzle was directed onto the surface of 10 mL of gMEM, prepared as described previously but without FBS to minimize foaming, in the collection vessel of an impinger (225-0020, SKC Inc.; Figure 3). For these tests, the nozzle airflow was again 16–17 L/min, but the nozzle fluid flow was increased to 0.4 mL/min in order to ensure a measurable viral titer was present in the collection medium. The increase in the fluid flow rate to the nozzle does not change the particle size distribution produced by the nozzle (see Supplementary Information), suggesting that stresses associated with generation are similar at the two flow rates. Aerosol generation lasted 45 s for each test to minimize evaporation of the collection fluid in the impinger, which was less than 10% of the initial volume based on the weights of the impinger recorded before and after each test. Initial testing using sodium fluorescein salt dissolved in PBS demonstrated complete recovery of material sprayed into the collection medium in the impinger jar, with an average recovery of 101.0 ± 2.5% using PBS as a collection medium ($n = 7$).

Results

Losses of viral infectivity for the different isolates of SARS-CoV-2, normalized for physical losses in the test system, are summarized in Figure 4 and Table 1. No significant differences were observed between any of the SARS-CoV-2 isolates or the different media combinations evaluated when compared by one-way ANOVA with a Tukey's multiple comparisons test ($P \geq 0.35$ for all comparisons). The average loss of infectivity pooled across all isolates and normalized for physical losses was −0.46 ± 0.17 $\log_{10}$ TCID_{50}/L-air, or 61 ± 15%. This loss was significantly different than zero when compared using a one-sample t-test ($P < 0.0001$).

As noted earlier, the initial droplet size distribution produced by the nozzle had a VMD of 6.2 μm and a GSD of 1.4 (see Supplementary Information). The final MMADs measured with the APS for tests with the different isolates of SARS-CoV-2 were between 1.3 and 1.6 μm (Table 1). These final sizes are similar to those reported for equilibrated particles exhaled by healthy individuals during quiet breathing (Holmgren et al. 2010; Johnson et al. 2011; Morawska et al. 2009). The values measured were also similar to those measured for tests with fluorescent tracer in PBS (MMAD: 1.42 ± 0.06 μm; GSD: 1.49 ± 0.03) that were used to normalize for physical losses in the test chamber.

To separate losses during aerosol generation from those occurring during evaporation, the output of the nozzle used for aerosol generation was collected directly onto the surface of the collection fluid in a liquid impinger. Average losses of viral infectivity for all isolates of aerosolized SARS-CoV-2 measured pre-evaporation were not significantly different between

any of the different isolates when compared by one-way ANOVA with a Tukey's multiple comparisons test ($P \geq 0.14$ for all comparisons). No loss of infectivity was observed for aerosolized virus collected pre-evaporation for any of the variants. The average loss across all variants was -0.04 ± 0.25 $\log_{10}$ $TCID_{50}$, which is not significantly different than zero when compared using a one-sample t-test ($P = 0.41$; $n = 18$) but is significantly less than the average loss measured for all isolates in equilibrated aerosol by the PTFE filters when compared using an unpaired t-test ($P < 0.0001$; Figure 5).

Discussion

Upon exhalation of respiratory particles into a lower humidity environment, water present in the particles is lost through evaporation, resulting in a decrease in particle size post-exhalation. The results of the present study demonstrate that a significant fraction of infectious SARS-CoV-2 is inactivated following aerosolization and evaporation at low RH in a flowing single-pass chamber. No loss of infectious virus was observed if the generated aerosol was collected immediately after exiting the nozzle but before particle evaporation and equilibration occurred, suggesting that the loss of infectivity occurred during the rapid evaporation of aerosol particles that occurs immediately post-generation. The loss of infectivity was similar for three different isolates of SARS-CoV-2, including isolates of the Delta and Omicron lineages, and averaged 61 ± 15% (-0.46 ± 0.17 $\log_{10}$ $TCID_{50}$). These results are in agreement with the 50–60% loss at RH levels below 50% reported recently by Oswin et al. (2022) in a series of experiments using an electrodynamic balance to trap aerosol particles containing earlier isolates of SARS-CoV-2 for periods ranging from 5 s to 20 min but extend their finding to include more recent variants of SARS-CoV-2. These results, together with a previous study from our laboratory which reported that the decay rates of different isolates of SARS-CoV-2 were similar in equilibrated aerosols over longer periods of time and across a range of environmental conditions (Schuit et al. 2021), suggest that it is not likely that an increase in environmental stability contributes to the observed increases in transmissibility observed with more recent variants of SARS-CoV-2. Additional studies are needed to explore other potential factors that could explain the observed increase in transmissibility, including differences in shedding from infected individuals and/or differences in the infectious dose of inhaled virus.

A significant and relatively rapid loss of viral infectivity post-exhalation suggests that the concentration of infectious aerosol may be higher in the vicinity of an infected individual before particle evaporation has occurred. It has been suggested that this brief period of greater infectivity may be another factor contributing to an increased potential for short-range disease transmission near an infected individual (Oswin et al. 2022). However, it should also be noted that the probability of infection following inhalation of an infectious bioaerosol is dependent not only on the concentration or amount of infectious material inhaled by a susceptible individual, but also the size distribution of the particles containing the micro-organism. Numerous studies have demonstrated that higher doses of an infectious bioaerosol, occasionally as great as several orders of magnitude, are needed to cause infection as particle size increases, likely due to a shift in the regional deposition to more proximal, better protected regions of the respiratory tract (Boydston et al. 2021; Day and Berendt 1972; Fitzgeorge et al. 1983; Sonkin 1949; Sonkin 1951; Wells 1955).

The size of exhaled particles would be expected to be larger during the brief period post-exhalation before evaporation and loss of viral infectivity occurs. Thus, it is possible that any increased risk associated with a higher concentration of infectious aerosol pre-evaporation may be offset by the increased particle size associated with these unevaporated particles. Unfortunately, data on the droplet size distributions of exhaled particles pre-evaporation, as well as the infectious dose of SARS-CoV-2 as a function of aerosol particle size are limited, complicating estimation of the relative probability of infection for these different scenarios (Chao et al. 2009). Additionally, it should be noted that the potential for disease transmission by exhaled particles is also dependent on numerous other factors, many of which are not well characterized, which complicates assessment of the impact of any one factor on transmission potential. These factors include the amount of virus shed by infected individuals, which has been reported to span multiple orders of magnitude in the exhaled breath and respiratory fluids of both symptomatic and asymptomatic COVID-19 patients (Malik et al. 2021; van Kampen et al. 2021; Wölfel et al. 2020; Yang et al. 2021), and the probability of infection as a function of the amount of infectious virus inhaled by an individual. While dose-response data have been reported previously for healthy adult nonhuman primates (Dabisch, Biryukov, et al. 2021), data on the influence factors such as age or comorbidities, as well as extrapolation to humans, are lacking.

In the present study, aerosols were generated from virus suspended in culture media, supplemented with either 2 or 10% FBS, and had a final equilibrated size similar to that reported for equilibrated particles exhaled during quiet breathing (MMAD <2 μm; NMAD <1 μm) (Holmgren et al. 2010; Johnson et al. 2011; Morawska et al. 2009). No difference was observed between media supplemented with different amounts of FBS. The study by Oswin et al. also utilized virus suspended in culture media, supplemented with 2% FBS, but utilized a larger particle size more representative of that expected to be expelled during a cough, with an equilibrated particle diameter of 10 to 20 μm (Johnson et al. 2011; Morawska et al. 2009; Oswin et al. 2022). Similar decreases in viral infectivity were observed in both studies despite this difference in size, suggesting that initial particle size may not greatly influence losses of SARS-CoV-2 infectivity that occur during particle evaporation, although additional studies designed to examine the influence of the initial droplet size on the survival of microorganisms during evaporation would be informative as particle size effects have been reported previously (Green and Green 1968). Numerous previous studies have examined the composition of respiratory fluids and exhaled particles, and several have noted changes in composition that occur in various disease states (Almstrand et al. 2010; Bicer 2015; Bredberg et al. 2012; Kumar et al. 2017; Larsson et al. 2012; Li and Tang 2021; Proctor and Shaalan 2021; Tinglev et al. 2016). Therefore, while the composition of the culture medium utilized in the present study has similarities to various respiratory fluids, additional studies are also needed to better characterize the composition of exhaled particles from COVID-19 patients and whether any disease-induced changes in composition may influence the losses of viral infectivity observed in evaporating particles.

Finally, it is possible that a portion of the observed losses of viral infectivity could occur during the aerosol sampling process, as numerous studies have demonstrated differences in the ability of different sampling devices to preserve the viability or infectivity of collected microorganisms. A previous study from our laboratory compared the performance of a

range of different aerosol sampling devices for sampling air-borne SARS-CoV-2 and found that the PTFE filters utilized in the present study are an efficient sampler for preservation of infectious virus. This study utilized SARS-CoV-2 suspended in simulated saliva and demonstrated the airborne concentration of infectious virus detected with PTFE filters was greater or equal to that measured by seven other low flow sampling devices. Additionally, unlike several of the other samplers tested, virus collected on PTFE filters remained infectious following periods of additional clean air flow through the filter post-collection (up to 30 min) that were much longer than those utilized in the present study (Ratnesar-Shumate et al. 2021). While these data don't eliminate the possibility that some of the observed loss of infectivity is occurring during the sampling process, it does provide confidence that such losses were minimized in the present study.

Supplementary Material

Refer to Web version on PubMed Central for supplementary material.

Acknowledgments

The authors thank Drs. Michael Hevey, Michael Schuit, and Louis Altamura for providing critical review and input, and Dr. Victoria Wahl for assistance acquiring the SARS-CoV-2 isolates from BEI Resources.

Funding

This work was supported by the DHS Science and Technology Directorate under agreement number HSHQDC-15-C-00064 to Battelle National Biodefense Institute for the management and operation of the National Biodefense Analysis and Countermeasures Center, a Federally Funded Research and Development Center (FFRDC).

References

Adenaiye OO, Lai J, Bueno de Mesquita PJ, Hong F, Youssefi S, German J, Tai S, Albert B, Schanz M, and Weston S 2022. Infectious severe acute respiratory syndrome coronavirus 2 (SARS-CoV-2) in exhaled aerosols and efficacy of masks during early mild infection. Clin. Infect. Dis. 75 (1):e241–48. [PubMed: 34519774]

Almstrand A-C, Bake B, Ljungström E, Larsson P, Bredberg A, Mirgorodskaya E, and Olin A-C 2010. Effect of airway opening on production of exhaled particles. J. Appl. Physiol 108 (3):584–88. doi:10.1152/japplphysiol.00873.2009. [PubMed: 20056850]

Benbough J 1967. Death mechanisms in airborne *Escherichia coli*. J. Gen. Microbiol 47 (3):325–33. doi:10.1099/00221287-47-3-325. [PubMed: 5340773]

Bicer EM 2015. Compositional characterisation of human respiratory tract lining fluids for the design of disease specific simulants. Doctoral diss., King's College London.

Bolze A, Luo S, White S, Cirulli ET, Wyman D, Dei Rossi A, Machado H, Cassens T, Jacobs S, and Schiabor Barrett KM 2021. SARS-CoV-2 variant delta rapidly displaced variant alpha in the United States and led to higher viral loads. Cell Rep. Med 3 (3):100564.

Bourouiba L 2020. Turbulent gas clouds and respiratory pathogen emissions: Potential implications for reducing transmission of covid-19. JAMA 323 (18):1837–38. doi:10.1001/jama.2020.4756. [PubMed: 32215590]

Bourouiba L, Dehandschoewercker E, and Bush JW 2014. Violent expiratory events: On coughing and sneezing. J. Fluid Mech 745:537–63. doi:10.1017/jfm.2014.88.

Boydston JA, Yeager JJ, Taylor JR, and Dabisch PA 2021. Influence of aerodynamic particle size on botulinum neurotoxin potency in mice. Inhal. Toxicol 33 (1): 1–7. doi:10.1080/08958378.2020.1851327. [PubMed: 33403871]

Bredberg A, Gobom J, Almstrand A-C, Larsson P, Blennow K, Olin A-C, and Mirgorodskaya E 2012. Exhaled endogenous particles contain lung proteins. Clin. Chem 58 (2):431–40. doi:10.1373/clinchem.2011.169235. [PubMed: 22156667]

Chao CYH, Wan MP, Morawska L, Johnson GR, Ristovski ZD, Hargreaves M, Mengersen K, Corbett S, Li Y, Xie X, et al. 2009. Characterization of expiration air jets and droplet size distributions immediately at the mouth opening. J. Aerosol Sci 40 (2):122–33. doi:10.1016/j.jaerosci.2008.10.003. [PubMed: 32287373]

Dabisch P, Schuit M, Herzog A, Beck K, Wood S, Krause M, Miller D, Weaver W, Freeburger D, Hooper I, et al. 2021. The influence of temperature, humidity, and simulated sunlight on the infectivity of SARS-CoV-2 in aerosols. Aerosol Sci. Technol 55 (2):142–53. doi:10.1080/02786826.2020.1829536. [PubMed: 38077296]

Dabisch PA, Biryukov J, Beck K, Boydston JA, Sanjak JS, Herzog A, Green B, Williams G, Yeager J, Bohannon JK, et al. 2021. Seroconversion and fever are dose-dependent in a nonhuman primate model of inhalational covid-19. PLoS Pathog 17 (8):e1009865. doi:10.371/journal.ppat.1009865. [PubMed: 34424943]

Day WC, and Berendt RF 1972. Experimental tularemia in *Macaca mulatta*: Relationship of aerosol particle size to the infectivity of airborne pasteurella tularensis. Infect. Immun 5 (1):77–82. doi:10.1128/iai.5.1.77-82.1972. [PubMed: 4632469]

Ferry RM, Brown WF, and Damon EB 1958. Studies of the loss of viability of bacterial aerosols*: III. Factors affecting death rates of certain non-pathogens. J. Hyg 56 (3):389–403. doi:10.1017/s0022172400037888. [PubMed: 13587989]

Fitzgeorge R, Baskerville A, Broster M, Hambleton P, and Dennis P 1983. Aerosol infection of animals with strains of legionella pneumophila of different virulence: Comparison with intraperitoneal and intranasal routes of infection. J. Hyg 90 (1):81–89. doi:10.1017/s0022172400063877. [PubMed: 6401778]

Green LH, and Green GM 1968. Direct method for determining the viability of a freshly generated mixed bacterial aerosol. Appl. Microbiol 16 (1):78–81. doi:10.1128/am.16.1.78-81.1968. [PubMed: 4865908]

Hess GE 1965. Effects of oxygen on aerosolized serratia marcescens. Appl. Microbiol 13 (5):781–87. doi:10.1128/am.13.5.781-787.1965. [PubMed: 5325941]

Holmgren H, Ljungström E, Almstrand A-C, Bake B, and Olin A-C 2010. Size distribution of exhaled particles in the range from 0.01 to 2.0 μm. J. Aerosol Sci 41 (5):439–46. doi:10.1016/j.jaerosci.2010.02.011.

Johnson GR, Morawska L, Ristovski ZD, Hargreaves M, Mengersen K, Chao CYH, Wan MP, Li Y, Xie X, Katoshevski D, et al. 2011. Modality of human expired aerosol size distributions. J. Aerosol Sci 42 (12): 839–51. doi:10.1016/j.jaerosci.2011.07.009.

Kumar A, Terakosolphan W, Hassoun M, Vandera K-K, Novicky A, Harvey R, Royall PG, Bicer EM, Eriksson J, Edwards K, et al. 2017. A biocompatible synthetic lung fluid based on human respiratory tract lining fluid composition. Pharm. Res 34 (12):2454–65. doi:10.1007/s11095-017-2169-4. [PubMed: 28560698]

Larsson P, Mirgorodskaya E, Samuelsson L, Bake B, Almstrand AC, Bredberg A, and Olin A-C 2012. Surfactant protein A and albumin in particles in exhaled air. Respir. Med 106 (2):197–204. doi:10.1016/j.rmed.2011.10.008. [PubMed: 22100538]

Lednicky JA, Lauzardo M, Alam MM, Elbadry MA, Stephenson CJ, Gibson JC, and Morris JG Jr. 2021. Isolation of SARS-CoV-2 from the air in a car driven by a covid patient with mild illness. Int. J. Infect. Dis 108: 212–16. doi:10.1016/j.ijid.2021.04.063. [PubMed: 33901650]

Lednicky JA, Lauzardo M, Hugh Fan Z, Jutla A, Tilly TB, Gangwar M, Usmani M, Shankar SN, Mohamed K, Eiguren-Fernandez A Jr., et al. 2020. Viable SARS-CoV-2 in the air of a hospital room with covid-19 patients. Int. J. Infect. Dis 100:476–82. doi:10.1016/j.ijid.2020.09.025. [PubMed: 32949774]

Li B, Deng A, Li K, Hu Y, Li Z, Shi Y, Xiong Q, Liu Z, Guo Q, Zou L, et al. 2022. Viral infection and transmission in a large, well-traced outbreak caused by the SARS-CoV-2 delta variant. Nat. Commun 13 (1):9. doi:10.1038/s41467-022-28089-y. [PubMed: 35013283]

Li Y, and Tang XX 2021. Abnormal airway mucus secretion induced by virus infection. Front. Immunol 12: 701443. doi:10.3389/fimmu.2021.701443. [PubMed: 34650550]

Liu L, Wei J, Li Y, and Ooi A 2017. Evaporation and dispersion of respiratory droplets from coughing. Indoor Air 27 (1):179–90. doi:10.1111/ina.12297. [PubMed: 26945674]

Ma J, Qi X, Chen H, Li X, Zhang Z, Wang H, Sun L, Zhang L, Guo J, Morawska L, et al. 2021. Coronavirus disease 2019 patients in earlier stages exhaled millions of severe acute respiratory syndrome coronavirus 2 per hour. Clin. Infect. Dis 72 (10):e652–54. doi:10.1093/cid/ciaa1283. [PubMed: 32857833]

Malik M, Kunze A-C, Bahmer T, Herget-Rosenthal S, and Kunze T 2021. SARS-CoV-2: Viral loads of exhaled breath and oronasopharyngeal specimens in hospitalized patients with covid-19. Int. J. Infect. Dis 110:105–10. doi: 10.1016/j.ijid.2021.07.012. [PubMed: 34242768]

Morawska L, Johnson G, Ristovski Z, Hargreaves M, Mengersen K, Corbett S, Chao CYH, Li Y, and Katoshevski D 2009. Size distribution and sites of origin of droplets expelled from the human respiratory tract during expiratory activities. J. Aerosol Sci 40 (3):256–69. doi: 10.1016/j.jaerosci.2008.11.002.

Moreira FRR, D'arc M, Mariani D, Herlinger AL, Schiffler FB, Rossi AD, Leitão IC, Miranda TDS, Cosentino MAC, Tôrres MCP, et al. 2021. Epidemiological dynamics of SARS-CoV-2 VOC Gamma in Rio de Janeiro, Brazil. Virus Evol 7 (2):veab087. doi: 10.1093/ve/veab087. [PubMed: 34725568]

Nicas M, Nazaroff WW, and Hubbard A 2005. Toward understanding the risk of secondary airborne infection: Emission of respirable pathogens. J. Occup. Environ. Hyg 2 (3):143–54. doi:10.1080/15459620590918466. [PubMed: 15764538]

Oswin HP, Haddrell AE, Otero-Fernandez M, Mann JFS, Cogan TA, Hilditch TG, Tian J, Hardy DA, Hill DJ, Finn A, et al. 2022. The dynamics of SARS-CoV-2 infectivity with changes in aerosol microenvironment. Proc. Natl. Acad. Sci. USA 119 (27):e2200109119. doi:10.1073/pnas.2200109119. [PubMed: 35763573]

Proctor G, and Shaalan A 2021. Disease-induced changes in salivary gland function and the composition of saliva. J. Dent. Res 100 (11):1201–09. doi:10.1177/00220345211004842. [PubMed: 33870742]

Ratnesar-Shumate S, Bohannon K, Williams G, Holland B, Krause M, Green B, Freeburger D, and Dabisch P 2021. Comparison of the performance of aerosol sampling devices for measuring infectious SARS-CoV-2 aerosols. Aerosol Sci. Technol 55 (8):975–86. doi:10.1080/02786826.2021.1910137. [PubMed: 38076006]

Schaffer F, Soergel M, and Straube D 1976. Survival of airborne influenza virus: Effects of propagating host, relative humidity, and composition of spray fluids. Arch. Virol 51 (4):263–73. doi:10.1007/BF01317930. [PubMed: 987765]

Schuit M, Biryukov J, Beck K, Yolitz J, Bohannon J, Weaver W, Miller D, Holland B, Krause M, Freeburger D, et al. 2021. The stability of an isolate of the SARS-CoV-2 B. 1.1.7 lineage in aerosols is similar to 3 earlier isolates. J. Infect. Dis 224:1641–48. doi:10.1093/infdis/jiab171. [PubMed: 33822064]

Schuit M, Ratnesar-Shumate S, Yolitz J, Williams G, Weaver W, Green B, Miller D, Krause M, Beck K, Wood S, et al. 2020. Airborne SARS-CoV-2 is rapidly inactivated by simulated sunlight. J. Infect. Dis 222 (4): 564–71. doi:10.1093/infdis/jiaa334. [PubMed: 32525979]

Smither SJ, Eastaugh LS, Findlay JS, and Lever MS 2020. Experimental aerosol survival of SARS-CoV-2 in artificial saliva and tissue culture media at medium and high humidity. Emerg. Microbes Infect 9 (1):1415–17. doi:10.1080/22221751.2020.1777906. [PubMed: 32496967]

Sonkin LS 1949. Infections induced in mice by local application of streptococci and pneumococci to the nasal mucosa and by intrapulmonary instillation. J. Infect. Dis 84 (3):290–305. doi:10.1093/infdis/84.3.290. [PubMed: 18127636]

Sonkin LS 1951. The role of particle size in experimental air-borne infection. Am. J. Hyg 53 (3):337–54. doi:10.1093/oxfordjournals.aje.a119459. [PubMed: 14829446]

Teyssou E, Delagrèverie H, Visseaux B, Lambert-Niclot S, Brichler S, Ferre V, Marot S, Jary A, Todesco E, Schnuriger A, et al. 2021. The delta SARS-CoV-2 variant has a higher viral load than

the beta and the historical variants in nasopharyngeal samples from newly diagnosed covid-19 patients. J. Infect 83 (4):e1–e3. doi:10.1016/j.jinf.2021.08.027.

Teyssou E, Soulie C, Visseaux B, Lambert-Niclot S, Ferre V, Marot S, Jary A, Sayon S, Zafilaza K, Leducq V, et al. 2021. The 501y. V2 SARS-CoV-2 variant has an intermediate viral load between the 501y. V1 and the historical variants in nasopharyngeal samples from newly diagnosed covid-19 patients. J. Infect 83 (1):119–45. doi: 10.1016/j.jinf.2021.04.023.

Theunissen H, Lemmens-den Toom NA, Burggraaf A, Stolz E, and Michel M 1993. Influence of temperature and relative humidity on the survival of chlamydia pneumoniae in aerosols. Appl. Environ. Microbiol 59 (8): 2589–93. doi:10.1128/aem.59.8.2589-2593.1993. [PubMed: 8368846]

Tinglev ÅD, Ullah S, Ljungkvist G, Viklund E, Olin A-C, and Beck O 2016. Characterization of exhaled breath particles collected by an electret filter technique. J. Breath Res 10 (2):026001. doi:10.1088/1752-7155/10/2/026001. [PubMed: 26987381]

van Doremalen N, Bushmaker T, Morris DH, Holbrook MG, Gamble A, Williamson BN, Tamin A, Harcourt JL, Thornburg NJ, Gerber SI, et al. 2020. Aerosol and surface stability of SARS-CoV-2 as compared with SARS-CoV-1. N. Engl. J. Med 382 (16):1564–67. doi:10.1056/NEJMc2004973. [PubMed: 32182409]

van Kampen JJA, van de Vijver DAMC, Fraaij PLA, Haagmans BL, Lamers MM, Okba N, van den Akker JPC, Endeman H, Gommers DAMPJ, Cornelissen JJ, et al. 2021. Duration and key determinants of infectious virus shedding in hospitalized patients with coronavirus disease-2019 (Covid-19). Nat. Commun 12 (1):6. doi:10.1038/s41467-020-20568-4. [PubMed: 33397903]

Wathes C, Howard K, and Webster A 1986. The survival of *Escherichia coli* in an aerosol at air temperatures of 15 and 30 °C and a range of humidities. J. Hyg 97 (3): 489–96. doi:10.1017/s0022172400063671. [PubMed: 3540114]

Webb S 1959. Factors affecting the viability of air-borne bacteria: I. Bacteria aerosolized from distilled water. Can. J. Microbiol 5 (6):649–69. doi:10.1139/m59-079.

Wells WF 1955. Airborne contagion and air hygiene. An ecological study of droplet infections. In Airborne contagion and air hygiene. An ecological study of droplet infections, ed. Cumberlege G, 117–122 and 352–371. London: Oxford University Press.

Wölfel R, Corman VM, Guggemos W, Seilmaier M, Zange S, Müller MA, Niemeyer D, Jones TC, Vollmar P, Rothe C, et al. 2020. Virological assessment of hospitalized patients with Covid-2019. Nature 581 (7809): 465–69. doi:10.1038/s41586-020-2196-x. [PubMed: 32235945]

Xie X, Li Y, Zhang T, and Fang HH 2006. Bacterial survival in evaporating deposited droplets on a teflon-coated surface. Appl. Microbiol. Biotechnol 73 (3):703–12. doi:10.1007/s00253-006-0492-5. [PubMed: 17053902]

Yang Q, Saldi TK, Gonzales PK, Lasda E, Decker CJ, Tat KL, Fink MR, Hager CR, Davis JC, Ozeroff CD, et al. 2021. Just 2% of SARS-CoV-2– positive individuals carry 90% of the virus circulating in communities. Proc. Natl. Acad. Sci. USA 118 (21): e2104547118. doi:10.1073/pnas.2104547118. [PubMed: 33972412]

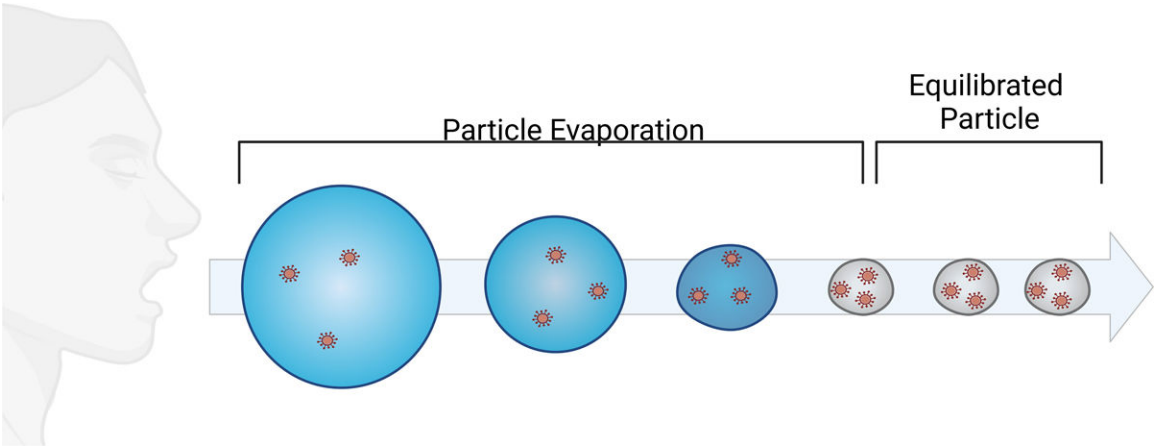

Figure 1.
Equilibration of exhaled particles. Created with Biorender.com.

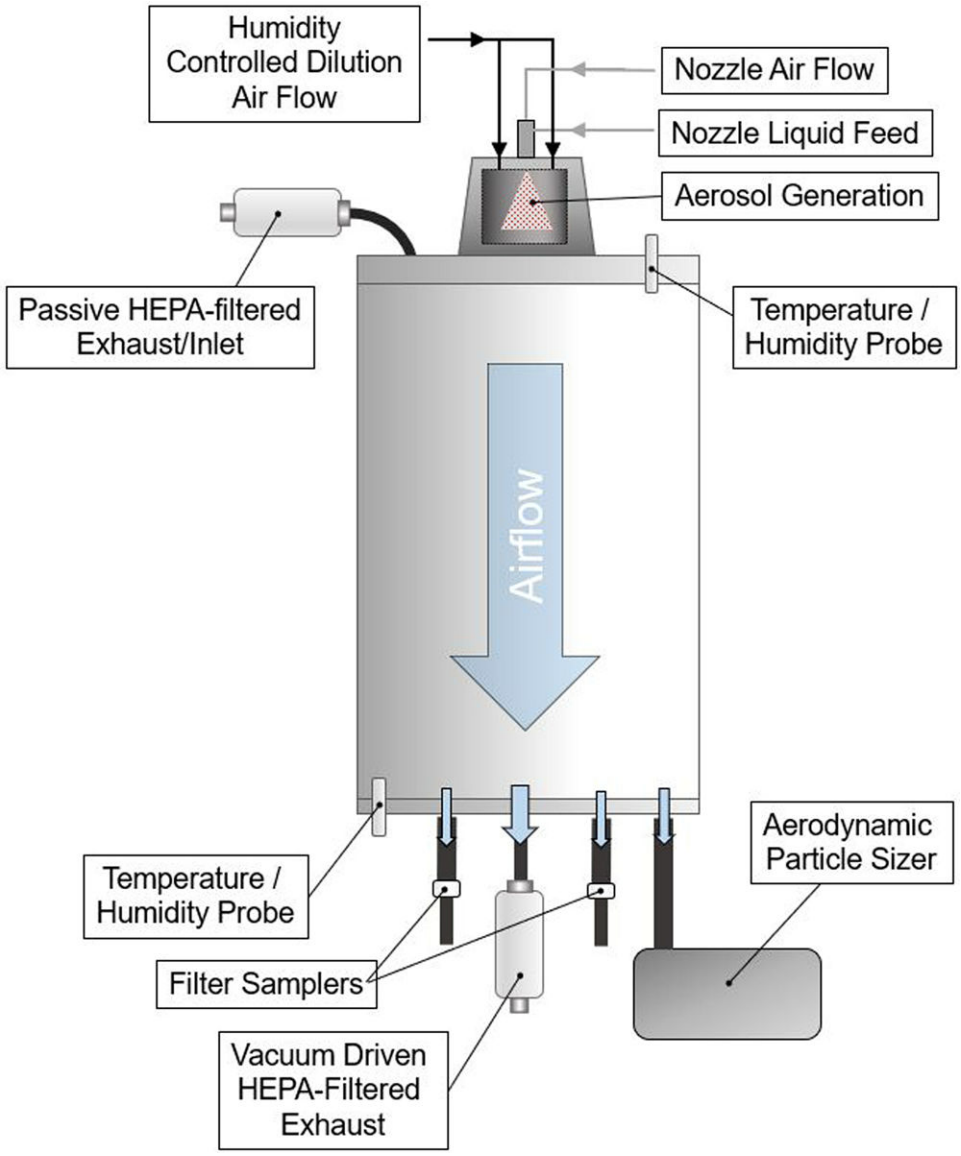

Figure 2.

Aerosol chamber schematic. The test system consisted of a cylindrical 67.5-L polycarbonate chamber supplied with room temperature humidity controlled air. Aerosol generation used an air assist nozzle attached to the top of the chamber that produced aerosol with an initial VMD of 6.3 μm and a GSD of 1.5. The generated aerosols were sampled from ports located at the distal end of the chamber using two 25-mm PTFE filters and an aerodynamic particle sizer (APS), all flowing at 5 L/min. The final equilibrated particle size distribution measured by the APS had an MMAD of 1.3–1.5 μm and a GSD of 1.5–1.6. An additional 40 L/min of exhaust flow was pulled from a separate HEPA-filtered port, resulting in a total exhaust flow of 55 L/min.

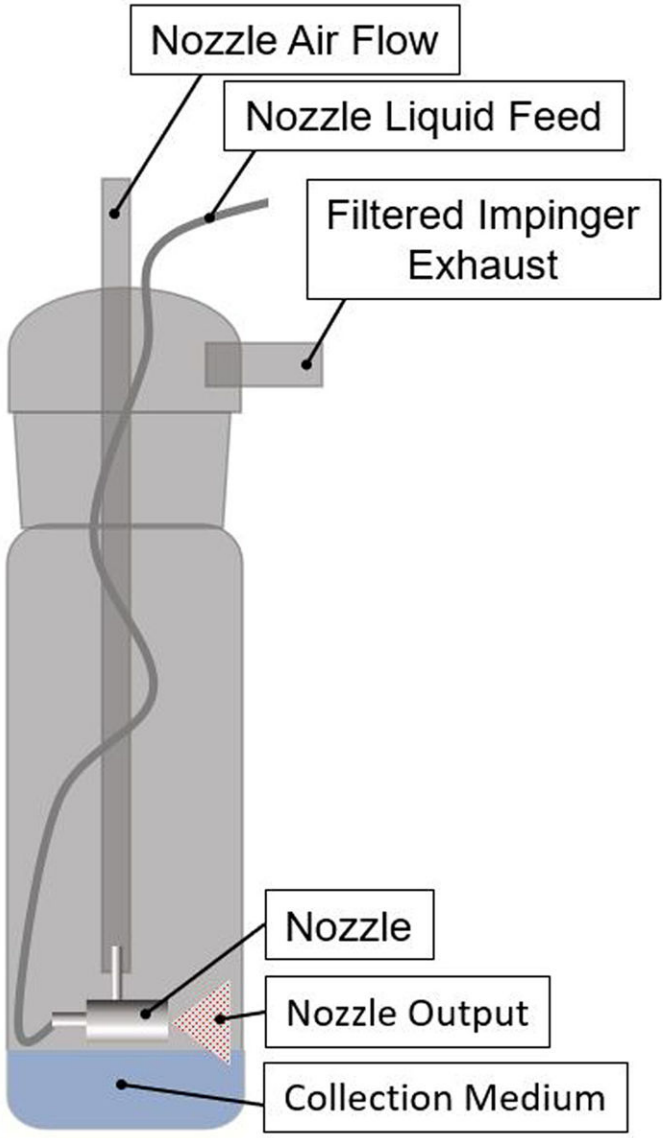

Figure 3.

Schematic of test system to evaluate losses of viral infectivity associated with the aerosol nozzle. To isolate losses during aerosol generation, the output of the nozzle used for aerosol generation was collected directly into an impinger containing ten mL of collection medium. For testing with virus, the collection medium was gMEM without FBS. Aerosol was generated for 45 s for each test. Airflow through the nozzle during the test resulted in evaporation of <10% of the collection medium in the impinger. Initial testing using a fluorescent tracer demonstrated complete recovery of material sprayed into the collection medium, with an average recovery of 101.0 ± 2.5% using PBS as a collection medium.

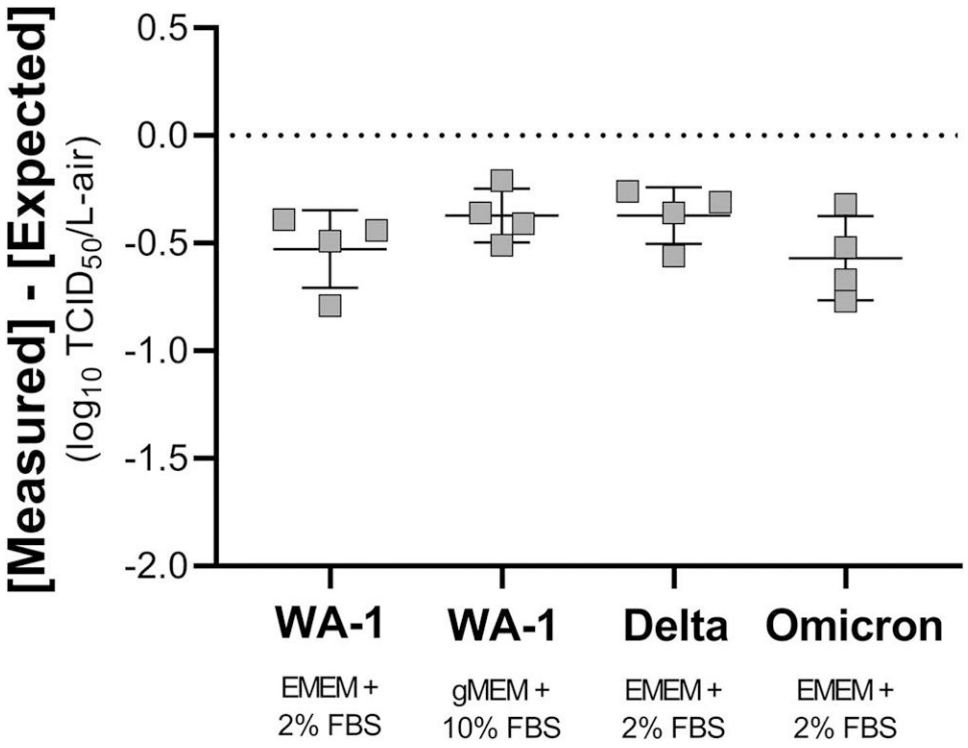

Figure 4.

Losses of infectivity of different isolates of SARS-CoV-2 in aerosol particles post-evaporation. Losses of viral infectivity for different variants of SARS-CoV-2, normalized for physical losses in the test system, are shown. No significant differences were observed between any of the isolates or suspension media evaluated ($P > 0.35$ for all comparisons). Squares represent the losses for each individual test, estimated as the average of the two PTFE filters sampling at 5 L/min. Lines represent the mean ± one standard deviation.

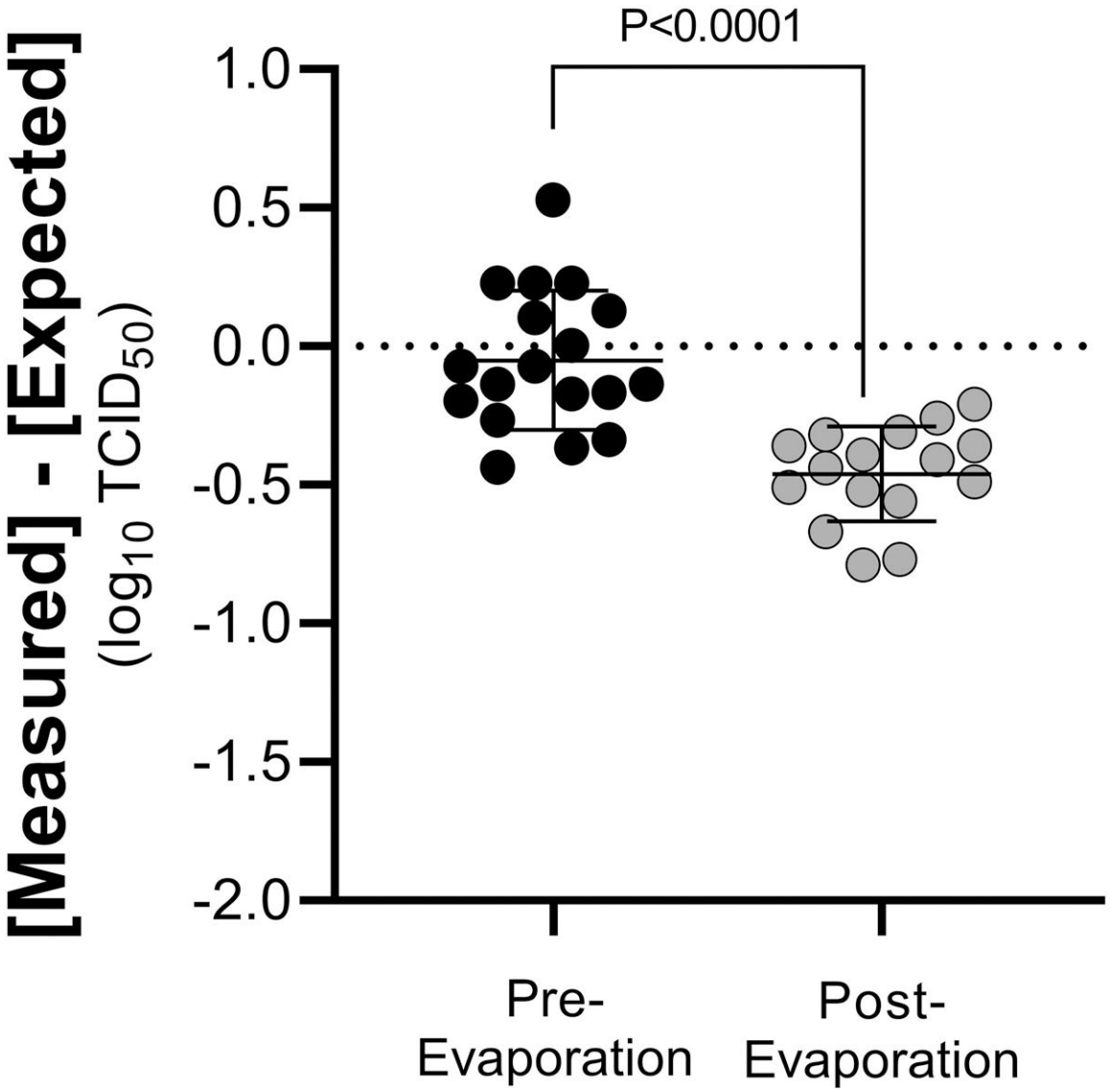

Figure 5.

Comparison of losses of SARS-CoV-2 infectivity in aerosol particle pre- and post-evaporation. Average losses of viral infectivity for all isolates of aerosolized SARS-CoV-2 measured pre-evaporation, following collection in a liquid impinger, and post-evaporation, following collection using PTFE filters, are shown. The average loss of viral infectivity measured pre-evaporation was −0.04 ± 0.25 $\log_{10}$ $TCID_{50}$, which was not significantly different than zero ($P = 0.41$). The average loss of viral infectivity measured post-evaporation, after normalizing for physical losses, was −0.46 ± 0.17 $\log_{10}$ $TCID_{50}$/L-air, significantly greater than the pooled value measured for the aerosol pre-evaporation ($P < 0.0001$).

Table 1.

Summary of infectivity losses and particle size statistics for different isolates of SARS-CoV-2 in aerosol particles post-evaporation.

	Loss in infectivity		Particle size statistics		
Suspension	**$\log_{10}$ loss ($TCID_{50}$/L-air)**	**Percentage loss**	**MMAD (μm)**	**GSD**	***n***
WA-1 in EMEM	−0.53 ± 0.18	−66 ± 11%	1.38 ± 0.07	1.62 ± 0.08	4
WA-1 in gMEM	−0.37 ± 0.13	−54 ± 16%	1.53 ± 0.02	1.56 ± 0.01	4
Delta in EMEM	−0.37 ± 0.13	−55 ± 12%	1.36 ± 0.01	1.54 ± 0.02	4
Omicron in EMEM	−0.57 ± 0.20	−69 ± 17%	1.44 ± 0.01	1.54 ± 0.03	4